Finite element failure analysis of wires for civil engineering applications with various crack-like laminations¡!–¡QUERY id="Q2" name="jrbendijo"¿¡ce:para¿Please provide affiliation for authors K. K. Adewole and S. J. Bull.¡/ce:para¿¡/QUERY¿–¿

K.K. Adewole, S.J. Bull

PII: S1350-6307(15)30164-3
DOI: doi: 10.1016/j.engfailanal.2015.11.043
Reference: EFA 2768

To appear in:

Received date: 21 June 2015
Revised date: 13 November 2015
Accepted date: 16 November 2015

Please cite this article as: Adewole KK, Bull SJ, Finite element failure analysis of wires for civil engineering applications with various crack-like laminations¡!–¡QUERY id="Q2" name="jrbendijo"¿¡ce:para¿Please provide affiliation for authors K. K. Adewole and S. J. Bull.¡/ce:para¿¡/QUERY¿–¿, (2015), doi: 10.1016/j.engfailanal.2015.11.043

Finite element failure analysis of wires for civil engineering applications with various crack-like laminations

K. K. Adewole and S. J. Bull

ABSTRACT

This paper presents the finite element (FE) failure predictions and analyses of a typical wire for civil engineering applications with various crack-like lamination types (Single and double), geometries (straight-end and inclined-end) and orientations (longitudinal, lateral and transverse). FE prediction and analysis of the failure of notched pre-cracked wires with a surface across-the-thickness crack-like lamination validated with experimental results is also presented. The FE predicted fracture shape for the notched pre-cracked wires that consists of a cup and cone fracture shape below the bottom tip of the surface across-the-thickness crack-like lamination agrees with the experimental fracture shape. Wires with the double straight-end and double inclined-end crack-like/line-type laminations exhibit a “slant-middle W” and a "zigzag" fractures respectively. Above and below the lateral mid-width across-the-thickness lamination, the wires with the lateral mid-width across-the-thickness lamination exhibits a combination of a transverse mid-thickness flat fracture that is perpendicular to the lateral mid-width across-the-thickness lamination and negatively inclined slant fractures on each side of the mid-thickness flat fracture at the remaining outer edges of the wire’s thickness. On both the front and back sides of the transverse mid-thickness across-the-width lamination, the wires with the transverse mid-thickness across-the-width lamination exhibits a combination of transverse flat fractures parallel to the transverse mid-thickness across-the-width lamination and positively inclined slant fractures at the outer edges of the wire’s thickness. FE failure analysis reveals that fracture initiations do not always begin at the termini of every longitudinal crack-like/line-type

lamination as reported in a published fractographic failure analysis report of wires with longitudinal crack-like laminations. Fracture initiation only begins at the termini/tip of longitudinal inclined-end crack-like laminations and at the termini/tip of transverse and lateral laminations. FE failure analysis also reveals that wires with single straight-end, double straight-end and double inclined-end longitudinal crack-like/line-type laminations do not exhibit cup and cone fractures as reported. This work further demonstrates the need to employ FE failure analysis as a complimentary or alternative failure analysis approach where the destruction/alteration of the fracture markings by corrosion could affect the accuracy of fractographic failure analysis.

Key words: Cup and cone fracture, Finite element failure analysis, Fracture behaviour, Crack-like lamination, Open-V fracture, Slant-middle W fracture, Wire, Zigzag fracture.

1.0 INTRODUCTION

The analysis of the failure of engineering structures is conducted to identify and understand the root cause of the failure to prevent recurrence and provide technical information for quality evaluation of engineering materials and components. The first step in failure analysis usually involves the macrofractographic or macroscopic examination for the classification of the fracture and the determination of the fracture origin/initiation point by tracing the fracture back to its starting point(s). Macrofractography, the examination of the detail on fracture surfaces with the unaided human eye (visual examination) or at low magnifications of <50x is considered the cornerstone, the first and the most efficient procedure for fracture evaluation/analysis [1]. This is followed by the microfractographic (microscopic) examination of important areas (e.g. fracture origin) selected during macroscopic examination at higher magnifications (above 50×) by light microscopy, scanning electron microscopy (SEM) etc. The microfractographic examination is done to: establish the fracture mode, confirm the fracture mechanism and detect features at the fracture origin. Finally, metallographic examination of the cross sections containing the origin is done to detect any microstructural features that promoted or caused fracture initiation, and determine if crack propagation is influenced by any microstructural constituent [1]. Visual examination of the fracture surface is performed for macroscopic classification of the fracture and for gaining an overall understanding of the fracture. Gaining an overall understanding of the fracture involves the location of the fracture origin(s), determination of the fracture sequence/propagation, and detection of any macroscopic features relevant to fracture initiation and/or propagation which are all essential for a successful/accurate failure analysis [1]. Locating the fracture origin (fracture initiation point) and determining the fracture propagation/sequence are the primary goals of fractography as they are vital to successful failure analyses and must be

determined in order to obtain conclusive failure analysis results [1]. Fracture origin/initiation and the fracture propagation/sequence are identified based on the characteristic fracture features/markings (such as river marks, radial lines, chevrons, or beach marks that indicate the direction of crack growth) formed during fracture which serve as the road map that the analyst uses to evaluate the fracture [1].

Both visual/macrofractographic and microfractographic/microscopic examinations involve studying of the fracture markings/features on the failure surfaces. Consequently, preserving the fracture markings/features is essential and all possible steps must be taken to ensure that the fracture features/markings are not obliterated or altered. Hence during failure investigation, it is imperative that the fracture face be handled carefully, avoiding excessive handling and touching of the fracture faces, and remating/fitting of the broken pieces together to prevent alteration/obliteration of the fracture markings/features. However, mechanical damage to the fracture surfaces may occur during crack propagation and such damage done to the main fracture may make successful microfractography and accurate failure analyses difficult. Also situations do arise in practice where the fracture surfaces, and invariably the fracture markings/features, are destroyed or drastically altered by the in-service failure incidents or by the post-fracture events (such as fire or corrosion). Such situations can often make a conclusive fracture interpretation and failure analysis difficult or impossible [1] and could lead to inaccurate failure analyses. Failure analysis is concluded by the interpretation of the results of the visual/macrofractographic, microfractographic/microscopic and metallographic examinations of the fracture surfaces to classify the fracture mode (ductile, brittle, fatigue, torsion etc), fracture mechanism (cleavage facets, ductile dimples, fatigue striations etc) and pinpoint any microstructural features that promoted or caused fracture initiation and/or favour fracture propagation [1].

The study of ductile failures is of considerable interest in quality control and materials evaluation. Tensile tests are conducted to determine materials tensile properties and tensile fracture behaviour. Tensile tests are conducted at room temperature, low strain rate, and in a dry environment, all of which favour ductile fracture [1]. The ideal tensile fracture is the classical cup-and-cone fracture with a flat fracture at the centre of the tensile specimen and two slant facture/shear lips inclined in opposite directions at the outer edges of the specimen [1 - 8]. For smooth (defect-free) specimens, the highest triaxial stresses develop at the centre of the necked section and not at the surface of the specimen, consequently, cup-and-cone fractures in smooth specimens begins with a flat fracture at the interior of the specimen and progresses to oppositely inclined slant fracture (along a shear band oriented at an angle of 50 to 60 ° from the transverse plane of the test specimen) toward the outer edge of the specimen [1-8].

The presence of longitudinal pre-service crack-like laminations in the pre-stressing wires of the Jordan Aqueduct pre-stressed concrete pipes has been found to be instrumental to the failure of the wires which led to the failure Jordan Aqueduct pre-stressed concrete pipes. Consequently, the need for the predictions of the effects of pre-service crack-like laminations on the fracture performance/behavior of wires used for civil engineering applications cannot be overemphasized. Laminations are elongated line-type defects or long cracks that are usually parallel to the surface of metal products produced through rolling or drawing process (e.g. wires) that constitute material separations or discontinuities [9 - 11].

1.1 Overview of the failure investigation of the ruptured Jordan Aqueduct pre-stressed concrete pipes conducted by the United States Department of Interior Bureau of Reclamation (USBR).

The USBR, (1994) [12] conducted holistic multidisciplinary failure investigations covering corrosion, design, petrographic, cathodic overprotection, structural, and metallurgical investigations as well as laboratory tensile testing of the pipe's pre-stressing wires to determine the cause(s) of the failure of the Jordan Aqueduct pre-stressed concrete pipes. The pipe failed just one month after putting the aqueduct into service. The USBR's (1994) [12] failure investigation revealed the following:

(a) Long, discontinuous, overlapping, and offsetting longitudinal cracks that typically ran through the entire 2-feet (600mm) length of all wire samples removed from the failed section of the pipe hereinafter referred to as longitudinal crack-like laminations were found in all examined wires from various locations along the aqueduct.

(b) The longitudinal crack-like laminations found in all examined pre-stressing wire samples were pre-service laminations as they were present in the pre-stressing wire at the time of pipe manufacture.

(c) The pre-service crack-like laminations were very straight for great lengths (up to several feet) in several coils of the wires.

(d) The pre-service crack-like laminations in the wires were not visible to the unaided eyes and some even remained invisible to the naked eyes after subjecting the wires to both the wrap test the bolt cutting test meant to reveal defects. The pre-service crack-like laminations were largely revealed by microscopic examinations as shown in Figures 1(a) to (c).

(e) No in-service/pre-failure corrosion of the pre-stressing wire surfaces at the failed pipe section was observed as the wires samples obtained from beneath the intact mortar at the failed section were untarnished. Only the fracture surfaces of the wires in the failed section of the pipe which were exposed by the failure event suffered incipient corrosion from atmospheric and ground

water effects with their surfaces covered with adherent layer of rust containing iron, oxygen, sodium, silicon, potassium, and calcium.

The USBR's (1994) [12] failure investigation conclusions are as follows:

(a) The longitudinal cracks prohibited the load from being carried uniformly across the cross section of the wire.

(b) Fracture initiations in the wires occurred and will always occur at the termini of the offsetting and overlapping pre-service longitudinal crack-like laminations as they are the locations of stress concentrations.

(c) Both the laboratory and field-fractured wires with pre-service crack-like laminations exhibited the fracture shapes shown in Figures 2(a) and (b) described as a cup and cone fracture combined with a sharp metal tongue formed by an offset between the ends of the overlapping and offsetting longitudinal cracks.

(d) The cup and cone failure were caused by overloading of the wire as the metal tongue/filament carried a "little load".

(e) With the exception of only one sample which failed below the required minimum tensile strength, all the longitudinally cracked wires subjected to laboratory tensile testing had ultimate tensile strengths above the required minimum strength.

(f) All the longitudinally cracked wires fractured with no measurable neck down and the offsetting longitudinal cracks was responsible for the small reductions in area as the longitudinally cracked wires cannot neck down normally like the un-cracked wires.

1.2 Deductions from of the USBR's (1994) [12] **report of the failure investigation of the ruptured Jordan Aqueduct pre-stressed concrete pipes**.

From the photomacrographs of the typical pre-service laminations in pre-stressing wires presented in the USBR's (1994) [12] report shown in Figures 1(a) to (c), the very straight long pre-service crack-like laminations end with inclined-end(s). As shown in Figures 1(a) and 2(b), in the very straight section of the crack-like laminations, the wires contained a single straight-end crack-like lamination and at the terminal of the single lamination, the wires contained a single inclined-end crack-like lamination as shown in Figure 1(c). Other sections of the wires contained inclined-end double offsetting and overlapping crack-like laminations with a metal tongue/ligament between the two offsetting and overlapping inclined-end crack-like laminations as shown in Figures 1(a), 1(b) and 2(a). The fracture shape exhibited by the section of the wire with the single straight-end crack-like lamination shown in Figure 2(b) was not identified in the USBR's (1994) [12] report and no information on its fracture process (fracture initiation and propagation) was presented in the report. As stated in the USBR's (1994) [12] report, the fractured surface of the wires exposed by the failure event suffered incipient corrosion with their surfaces covered with an adherent layer of rust. This technically means that the microscopic examinations of the field-fractured wire surfaces conducted by USBR, (1994) [12] were conducted on corroded fractured wire surfaces. As state earlier, post-fracture events, such as the corrosion of the pipe's pre-stressing wire surfaces observed by USBR (1994) [12] leads to the destruction or drastic alteration of the fracture markings/features necessary for successful/accurate fractographic failure analyses which could make successful/accurate fractographic failure analyses difficult or impossible. It is unclear if USBR (1994) [12] conducted microscopic fractographic examinations of the un-corroded surface of the laboratory-fractured wire that exhibited the same fracture shapes as the field-fractured wires shown in Figures 2(a) and (b) as the evidence(s) of the microscopic fractographic examinations of the

laboratory-fractured un-corroded wire surfaces were not presented in the failure analysis report of the USBR (1994) [12].

In this paper, the analyses of the failures of typical wires for civil engineering applications with various lamination types (single and double), geometries (straight-end and inclined end) and orientations (longitudinal, lateral and transverse) using finite element (FE) analysis are presented. The FE failure analyses covers the predictions and analyses of the failures of notched pre-cracked wire, and the wires with longitudinal double straight-end, longitudinal double inclined-end; lateral mid-width across-the-thickness and transverse mid-thickness across-the-width laminations. For a holistic comparison of the effects of the various crack-like lamination types, geometries and orientations on the wires tensile properties and fracture behaviours, the comparisons of the tensile properties and the fracture behaviors of the lamination-free wires and the wire with the longitudinal single straight-end lamination earlier published by the authours (see Adewole and Bull, 2014a [12]) are also presented. The comparisons of the predicted fracture processes and fracture shapes of the wires with the longitudinal single straight-end and the wire with the longitudinal double inclined-end laminations, typically found in the fractured pres-stressing wires of Jordan Aqueduct pre-stressed concrete pipes with that presented in the published Jordan Aqueduct pre-stressed concrete pipe pres-stressing wires fractographic failure analysis report are also presented.

The flat wires considered in this work are employed as tensile armour wires and/or pressure armour wires that are incorporated into flexible pipes to provide the pipe's resistance to axial and/or hoop stresses. Flexible pipes are used as flowlines and risers for offshore oil and gas transportation. The presence of laminations in wires for civil engineering applications generally is a concern which explains why the tensile and pressure armour wires are subjected to reverse

bending and straitening tests [13] and why the pres-stressing wires are subjected to both wrap and bolt cutting test [1] to reveal laminations in the wires. The crack-like/line-type laminations considered in this work are the types found in the fractured Jordan Aqueduct pre-stressed concrete pipes pre-stressing wires that are not visible to the unaided eyes and even remained invisible to the naked eyes after subjecting the wires to the reverse bending and straitening test, the wrap test and/or the bolt cutting test [1, 13].

2.0 Finite element tensile fracture simulation and validation

The FE failure analysis in this work covers the prediction and the analysis of the failure of the experimental wire specimens with a 2mm deep 60^0 V-notch and a 1mm deep surface lateral across-the-thickness crack-like lamination shown in Figure 3(a) hereinafter simply referred to as the notched pre-cracked wire. The FE model of the notched pre-cracked wire model is presented in Figure 3(b). Details of the pre-cracking procedure and the experimental tensile testing of the notched pre-cracked wire specimens can be obtained from the published work of the author (see Adewole and Bull, 2013[b] [15]). The FE failure analysis also covers the predictions and the analyses of the failures of the wires with 5-15mm long longitudinal double straight-end and double inclined-end laminations; and the wires with 0.5 to 2.5mm deep lateral mid-width across-the-thickness and transverse mid-thickness across-the-width laminations.

The crack-like/line-type laminations considered are not visible in the meshed wire models. Consequently, they are presented in the unmeshed models in Figures 3(c) to (g). As shown in Figure 3(d), the left end of the back inclined-end crack-like lamination is inclined at 45º to the z-axis (i.e. positive 45º inclination to z-axis), while the right end of the front inclined-end crack-like lamination is inclined at 135º to the z-axis (i.e. negative 45º inclination to z-axis) similar to the inclined-end crack-like laminations found in the pre-stressing wire in Figure 2(a). The

lengths of the inclined ends varied from 0.5mm to 1mm. The FE tensile fracture simulations were conducted on mid-gauge length longitudinal across-the-width crack-like laminations with lengths from 5 to 15mm (30% of gauge length). The overlaps between the double overlapping and offsetting longitudinal crack-like laminations were varied from 5 to 10mm and the thickness of the filament/metal tongue between the double overlapping and offsetting longitudinal crack-like laminations were varied from 0.5mm to 1.5mm and 0.5mm to 2.1mm for the 12mm x 5mm and 12mm x 7mm wires respectively. 1.5mm and 2.1mm represent 30% of the thicknesses of 12mm x 5mm and 12mm x 7mm wires respectively. The 0.5 to 2.5mm depths of the lateral across-the-thickness and the transverse across-the-width laminations are in the wire's width (conventional Y-axis) and thickness (conventional Z-axis) directions respectively. The lengths of the lateral across-the-thickness and the transverse across-the-width laminations cut across the wires' thickness and width respectively.

As shown in Figure 3(b), the tensile fracture simulation was conducted by fixing the left hand end of the models and pulling the right hand end which is free to move only in the wire's longitudinal direction until the wires fractured. The middle region of the wire models were meshed with fine 0.1mm x 0.1mm x 1mm elements, while the outer regions were meshed with coarse 1mmx1mmx1mm C3D8R (8-node linear brick, reduced integration, hourglass control) elements positioned with the elements length in the wire width as shown in Figure 3(b). The mesh design employed for these simulations has been established in the earlier work of the author (see Adewole (2014c) [16]) to be the appropriate mesh design for accurate predictions of the tensile and fracture behaviours of the wires considered in this work. The crack-like/line-type laminations were modelled as seams (partition lines which open during analysis), a modelling

approach that has been established by [17] as an appropriate simulation technique for modelling crack-like/line-type laminations.

The FE simulations were conducted with the true yield stress and true plastic strain at yield, and the true ultimate tensile stress and true plastic strain at the ultimate strength of the wires obtained experimentally. Interested readers are referred to Adewole and Bull, [13, 16, 17 for the details of the laboratory tensile fracture test conducted on the wires to obtain the tensile properties of the wire employed for the simulations conducted in this work. The values of the yield stress, the ultimate stress and their corresponding strains as well as the displacements at fracture of the 12mm x 5mm and 12mm x 7mm wire sizes considered are not presented in this work for confidentiality purposes (due to the non-disclosure agreement on the tensile properties of the wire made with the flexible pipe manufacture that supplied the wires).

The tensile fracture simulations were conducted with the isotropic elastic-plastic and micromechanical-based phenomenological shear damage and fracture models, which have been established by Adewole [18] as a model combination for the accurate predictions of the tensile and fracture behaviours of the tensile/pressure armour wires considered in this work. Interested readers are referred to Adewole [18] for the details of the models and their modelling parameters. The calibrated phenomenological shear damage and fracture model parameters employed in this work are equivalent plastic strain at onset of shear damage of 0.3451, shear stress ratio of 12.5, strain rate of $0.000125s^{-1}$, material parameter, K_s of 0.3 and plastic displacement at failure of 0.2 obtained through phenomenological curve fitting procedures in the earlier work of the authours (see Adewole [18]). The calibrated phenomenological shear damage and fracture model parameters employed in this work were obtained through the phenomenological curve fitting procedures because obtaining the calibrated parameters for micromechanical fracture modelling

experimentally through metallurgical and material testing are generally extensive and expensive [19] Specifically, obtaining the phenomenological shear damage and fracture model parameters through experimentation requires conducting extensive experiments over a range of shear stress ratio with specially designed specimens, the details of which are presented in [19, 20]. This explains why the calibrated parameters for micromechanical fracture modelling are predominantly obtained through the phenomenological curve fitting process [19, 21].

The phenomenological fitting procedure is conducted by keeping some parameters constant while varying others until the FE simulation predicts the same displacement at fracture as the experimental value. The values of the set of damage and fracture parameters at which the predicted displacement at fracture agrees with the experimental displacement at fracture are generally taken as the calibrated fracture parameters [19]. The calibrated phenomenological shear damage and fracture model parameters employed in this work are not the measured parameters of the wires but were rather obtained as the values of the set of damage and fracture parameters at which the FE predicted displacement at fracture equaled/agreed with the experimental displacement at fracture of the wires. Thus, the experimental true yield stress and true plastic strain at yield, and the true ultimate tensile stress and true plastic strain at the ultimate strength of the wires were employed for the predictions of the elastic and the plastic behaviours of the wires, while the experimental displacements at fracture of the wires were employed for the calibration of the phenomenological shear damage and fracture model parameters employed in the FE failure simulations.

3.0 Result

The predicted deformed shapes throughout the tensile fracture simulations conducted on the wires with the varying 5mm to 15mm long longitudinal double laminations and on the wires with

the varying 0.5 to 2.5mm deep lateral mid-width across-the-thickness and transverse mid-thickness-across-the-width laminations are the same. Consequently, only the deformed shapes throughout the tensile fracture simulations predicted by the simulations conducted on the wires with the 15mm long longitudinal double laminations and the wires with the 2mm deep lateral mid-width across-the-thickness and transverse mid-thickness across-the-width crack-like laminations are presented. Only the predicted fracture shapes of the lamination-free wire and the wire with the longitudinal single straight-end lamination are presented as their detailed fracture processes have been presented in the earlier published work of the authours (see Adewole and Bull, [13]).

The FE predicted deformed shapes at the various stages of the deformation of the notched pre-cracked wire specimen with the surface lateral across-the-thickness lamination at the tip of the notch are presented in Figures 4(a) to (j). The experimental fractured notched pre-cracked wire is shown in Figure 4(k). The FE predicted deformed shapes for the wires with the longitudinal double inclined-end, longitudinal double straight-end, lateral across-the-thickness and transverse across-the-width crack-like laminations at the end of the elastic deformation (prior to yielding, where the stress concentration effect is most significant), at the end of the uniform plastic deformation (prior to necking), and at the end of the necking process are shown in Figures 5 to 7. The FE predicted deformed shapes for the wires with the longitudinal double inclined-end, longitudinal double straight-end, lateral mid-width across-the-thickness and transverse mid-thickness across-the-width crack-like laminations at the various stages/processes of the wires are presented in Figures 8 to 14. For an holistic comparison of the effects of the various lamination types and orientations on the wire's fracture processes and shapes, the predicted fracture shapes and the experimental or field/in-service fracture shapes of the lamination-free wire and the wire

with the longitudinal single straight-end crack-like lamination presented in the earlier work of the Authours (see Adewole and Bull, [13]) are also presented in Figures 15 (a) to (d). The predicted fractured and the field/in-service fractured wires with the longitudinal double inclined-end crack-like laminations are presented in Figures 15(e) and (f) respectively. The force-displacement curves for the lamination-free wire and the wires with laminations are presented in Figures 16.

5.0 Discussion

Only the experimental validation of the simulation of the tensile fracture behavior (fracture process and fracture shape) of the notched pre-cracked wires with the surface lateral across-the-thickness crack-like lamination below the tip of the V-notch that can be experimentally machined or introduced into the wire by the fatigue/cyclic loading process was conducted. The experimental validations of the simulations of the tensile fracture behaviors of the wires with the longitudinal double inclined-end, longitudinal double straight-end, lateral mid-width across-the-thickness and transverse mid-thickness across-the-width laminations considered in this work could not be conducted. This is due to the fact that it is experimentally impossible to machine these various crack-like lamination types, geometries and orientations into the wire specimens at the locations considered. However, the ability of the simulation technique employed in this work that was employed in the earlier work of the authours (see Adewole and Bull [13]) to accurately predict the fracture shapes of the lamination-free wires (Figures 15(a)) and the wire with the single straight-end lamination (Figures 15(c)) that agrees with the experimental fracture shapes presented in Figures 15(b) and (d) respectively demonstrates the accuracy of the FE failure simulations presented in this work. The predictions of the force-displacement curve (Figure (16)) and the fracture shape of the V-notched pre-cracked wire with the surface lateral across-the-

thickness crack-like lamination (Figure 4(j)) presented in this work that agrees with the experimental fracture shape (Figure 4(k)) also demonstrates the accuracy of the FE failure predictions conducted in this work. The prediction of the fracture shape of the wire with the double inclined-end lamination (Figure 15(e)) that agrees well with the fracture shape of the field/in-service-fractured wire shown in Figure 15(f) further demonstrates the accuracy of the FE failure predictions presented in this work.

As stated in section 1, the introduction section, laminations constitute material separations. Consequently, all the lamination types considered divided/split the wire at their various locations. The surface lateral across-the-thickness crack-like lamination split the section of the wire below the V-notch tip into the right and left sections. At the peak of the elastic deformation prior to yielding, at the ultimate tensile strength (i.e. at the commencement of necking) and at the end of the necking process, the notched pre-cracked wire exhibited non-uniform stress distributions and openings as shown in Figures 4(a), (b) and (c) respectively. The highest stress occurred at the bottom tips of the surface lateral across-the-thickness crack-like lamination due to the stress concentration at its bottom tip. The stress concentration at the bottom tip of the surface lateral across-the-thickness crack-like lamination resulted from the interruption/disruption of the tensile load path in the wire's longitudinal direction by the surface lateral across-the-thickness crack-like lamination due to its perpendicularity to the tensile load path.

The openings at the location of the surface lateral across-the-thickness lamination below the V-notch tip shown in Figures 4(a), (b) and (c) resulted from the widening of the straight 2mm separation created by the lamination by the longitudinal tensioning of the wire which pulled the right and left sections of the separated section of the notched pre-cracked wire apart. The pointed

bottom end of the opening resulted from the simultaneous anticlockwise and clockwise rotations of the elements at the bottom tips of the left and right sections of the separation created by the lamination respectively. The rotations of the elements at the bottom tips of the across-the-thickness surface lamination rather than the propagation of the crack-like lamination resulted from the stress redistribution at the lamination tips and the lamination tips blunting usually associated with ductile metals such as the steel wire considered. The straight vertical section of the opening resulted from the longitudinal displacement of the remaining straight sections of the 2mm long surface lateral across-the-thickness crack-like lamination by the tensioning of the wires. As shown in Figures 4(a) to (c), the widening of the opening continued up to the point of fracture initiation shown in Figure 4(d). As shown in Figure 4(d), the fracture of the notched pre-cracked wire began with a mid-thickness flat fracture at the pointed tip of the opening because the highest triaxial stress occurred at this location. This was followed by the simultaneous vertical/transverse downward flat fracture propagation in the middle half of the wire's thickness along the wire's width and the lateral frontward and backward propagations of the flat fracture along the wire's thickness as shown in Figure 4(e). The flat fracture covering approximately the middle half of the wire's thickness continued to propagate vertically downward along the wire's width while the lateral frontward and backward flat fracture propagations transited to a positively and a negatively inclined slant fractures at the outer back and the outer front sections of the wire's thickness respectively as shown in Figure 4(f). The fracture proceeded with the simultaneous vertical downward propagation of the mid-thickness flat fracture and the frontward and backward slant fracture propagations as shown in Figure 4(g). As shown in Figure 4(h), the vertical downward flat fracture propagation continued while the oppositely inclined slant fractures propagated to the back and front faces of the wire leading to the formation of the cup

and cone fracture in the region of the wire immediately below the lamination/opening's bottom tip that is now visible in the meshed model shown in Figure 4(h). The cup and cone fracture as stated in the introduction section consists of a middle flat fracture and oppositely inclined slant fractures at the outer regions of tensile specimens. The fracture of the notched pre-cracked wire continued with the all the aforementioned fracture stages/steps that led to the cup and cone fracture formation leading to the propagation the cup and cone fracture vertically downward through the wire's width (Figure (4i)). This leaves the V-notched pre-cracked wire with the surface lateral across-the-thickness crack-like lamination with a cup and cone fracture shape below the surface lateral across-the-thickness crack-like lamination as shown in Figure 4(j) that agrees with the fracture shape exhibited by the experimental fractured notched pre-cracked wire shown in Figure 4(k).

The longitudinal double straight-end laminations and the straight section of the longitudinal double inclined-end crack-like laminations divided the wire into three ligaments hereinafter referred to as the front, the middle and the back ligaments. The inclined section of the double inclined-end laminations, the lateral mid-width across-the-thickness and the transverse mid-thickness across-the-width laminations divided the wires into two sections hereinafter referred to as the left and the right sections. At the peak of the elastic deformation (prior to yielding), at the ultimate tensile strength (prior to necking) and at the end of the necking process, the wires with the longitudinal double inclined-end, lateral mid-width across-the-thickness and transverse mid-thickness across-the-width crack-like laminations exhibited non-uniform stress distributions and openings as shown in Figures 5(a), (c) and (d), Figures 6(a), (c) and (d)) and Figures 7(a), (c) and (d)) respectively. Conversely, the wire with the longitudinal double straight-end crack-like laminations exhibited a uniform stress distribution and exhibited openings only at the end of the

necking process (Figures 5(b), 6(b) and 7(b)). The highest stress occurred at the tips of the inclined end of the double inclined-end crack-like longitudinal laminations and at the tips of the lateral mid-width across-the-thickness and transverse mid-thickness across-the-width crack-like laminations due to the stress concentrations at the tips of the crack-like laminations.

The wire models with the double straight-end crack-like longitudinal laminations exhibit uniform stress distributions and no stress concentration because the longitudinal crack-like laminations are parallel to the load path (wire's longitudinal direction) and do not interrupt/obstruct the load path and the stress distributions. The wire model with the longitudinal double inclined-end, lateral mid-width across-the-thickness and transverse mid-thickness across-the-width crack-like laminations exhibit stress concentrations because the crack-like laminations in the wire with the double inclined-end lamination, and the wires with the lateral mid-width across-the-thickness and transverse mid-thickness across-the-width crack-like laminations that are inclined to and perpendicular to the load path respectively interrupt/obstruct the load path. The non-uniform stress distribution exhibited by the wire with the longitudinal double inclined-end lamination agrees with the conclusion of USBR [12] that the longitudinal cracks prohibited the load from being carried uniformly in all areas of the fracture. However, this conclusion is only true for the wires with the longitudinal double inclined-end, lateral mid-width across-the-thickness and transverse mid-thickness across-the-width crack-like laminations as the wires with the double straight-end longitudinal laminations exhibited uniform stress distribution. This implies that the wires with the longitudinal double straight-end laminations were subjected to uniform loading throughout their cross-sections.

As shown in Figures 5 to 7, the wires with the longitudinal double inclined-end, lateral mid-width across-the-thickness and transverse mid-thickness across-the-width crack-like laminations

exhibited openings from the beginning of the tensile fracture simulation to the end of the necking processes. Conversely, the wire with the longitudinal double straight-end crack-like laminations exhibited openings only during the necking process. The longitudinal double inclined-end laminations exhibited two opening shapes with the two inclined sections exhibiting triangular-shaped openings while the two straight portions widened laterally as shown in Figures 5(a), 6(a) and 7(a). Conversely, the entire longitudinal double straight-end laminations widened laterally as shown in Figure 7(b). As shown in Figures 5(c), 6(c) and 7(c), the wire with the lateral mid-width across-the-thickness lamination exhibited a vertical hexagonal-shaped opening with the two acute angles of the hexagonal-shaped opening pointing in the wire's width (Y-axis) direction. Similarly, as shown in Figures 5(d), 6(d) and 7(d), the wire with the transverse mid-thickness across-the-width lamination exhibited a horizontal hexagonal-shaped opening with the two acute angles of the hexagonal-shaped opening pointing in the wire's thickness (Z-axis) direction.

The triangular-shaped openings exhibited by the inclined ends of the longitudinal double inclined-end crack-like laminations resulted from the simultaneous anticlockwise and clockwise rotations of the elements at the tip of the left and right sections of the separated section of the wire at the inclined ends of the inclined-end laminations. Throughout the entire length of the longitudinal double straight-end laminations and the straight section of the inclined-end crack-like laminations, the separate contraction and necking of the three ligaments led to the backward transverse contraction of the edge of the back ligament, the frontward transverse contraction of the edge of the front ligament, and both backward and frontward lateral contractions in the middle ligament. This resulted into the two openings (one between the back and the middle ligaments, and the other between the front and the middle ligaments) at the locations of the

straight section of the longitudinal double inclined-end laminations and across the entire length of the double straight-end crack-like laminations as shown in Figures 7(a) and (b).

The hexagonal-shaped openings exhibited at the locations of the lateral mid-width across-the-thickness and the transverse mid-thickness across-the-width line-type laminations also resulted from the simultaneous rotations of the two elements at the top and bottom tips, and at the front and back tips of the lateral mid-width across-the-thickness and the transverse mid-thickness across-the-width line-type laminations respectively and the longitudinal displacement of the remaining straight sections of the 2mm long laminations. As earlier stated, the rotations of the elements at the tips of the double inclined-end, the lateral mid-width across-the-thickness and the transverse mid-thickness across-the-width line-type laminations rather than the propagation of the crack-like laminations resulted from the stress redistribution at the lamination tips and the lamination tips blunting.

Thus, the creations of the openings at the locations of: the inclined end of the longitudinal double inclined-end, the lateral mid-width across-the-thickness and the transverse mid-thickness across-the-width crack-like laminations resulted largely from the tensile dilation/widening of the separations created by these lamination types by the applied tensile load. Conversely, the creations of the openings at the locations of the straight portions of the longitudinal double inclined-end and across the entire length of the double straight-end crack-like laminations resulted from the lateral backward and frontward contractions of the front, the back and the middle ligaments.

The first fracture stage in the wire with the longitudinal double inclined-end crack-like laminations involved two slant fracture initiations each at the tips of the inclined end of the

inclined-end crack-like laminations as shown in Figures 8(a). The first fracture stage in the wire with the longitudinal double straight-end crack-like laminations involved a single flat fracture initiation in the middle ligament of the wire as shown in Figures 8(b). The first fracture stage in the wire with the lateral mid-width across-the-thickness lamination involved two mid-thickness flat fracture initiations each at the top and the bottom tips of the vertical hexagonal-shaped opening in the wire as shown in Figures 8(c). Similarly, the first fracture stage in the wire with the transverse mid-thickness across-the-width lamination involved two mid-width flat fracture initiations each at the front tip and the back tip of the horizontal hexagonal-shaped opening in the wire as shown in Figures 8(d).

The fracture of the wire with the longitudinal double inclined-end laminations began with slant fracture initiations at the tips of the inclined-ends and not at the tip of the straight end of the longitudinal inclined-end crack-like laminations. This is due to the fact that the highest stress occurred at the tips of the inclined-ends of the longitudinal inclined-end crack-like laminations due to the stress concentration effect of the inclined-end of the longitudinal inclined-end laminations. Conversely, the fracture of the wire with the longitudinal double straight-end laminations began with a single flat fracture initiation at the centre of the middle ligament and not at the tips of the longitudinal double straight-end laminations because the highest triaxial stress caused by necking occurred at the centre of the middle ligament. Also the fracture of the wire with the longitudinal double inclined-end laminations began at the regions of the back and front ligaments next to the tip of the longitudinal inclined-end laminations and not at the centre of the front, back or middle ligaments as shown in Figure 8(a). This is due to the fact that the highest stress occurred at the regions of the back and front ligaments next to the tips of the inclined-end of the longitudinal inclined-end laminations due to the stress concentration effects

of the inclined-end of the longitudinal inclined-end laminations. Conversely, the fracture of the wire with the longitudinal double straight-end laminations began at the centre of the thinner 1mm middle ligament (Figure 8(b)) and not at the centre of any of the two 3mm thicker front and back ligaments because the highest stress occurred at the middle of the 1mm middle ligament due to its smaller size. The fracture of the wires with the lateral mid-width across-the-thickness and transverse mid-thickness across-the-width laminations started at the tips of the hexagonal-shaped openings because the highest stress occurred at these locations due to the stress concentration effect of pointed ends of the hexagonal-shaped openings.

The second fracture stage in the wire with the double inclined-end crack-like laminations involved the propagation of the slant fracture at the tip of each of the inclined ends of the inclined-end crack-like laminations frontward and backward through the wires thickness as shown in Figure 9(a). Conversely, the second fracture stage in the wire with the double straight-end crack-like laminations involved the upward and downward vertical propagations of the initiated single flat fracture in the middle ligament along the wire's width as shown in Figures 9(b). The second fracture stage in the wire with the lateral mid-width across-the-thickness lamination involved the simultaneous transverse and lateral propagations of the initiated flat fracture upward and downward along the wire's width, and frontward and backward along the wire's thickness respectively above and below the lateral mid-width across-the-thickness lamination as shown in Figure 9(c). Similarly, the second fracture stage in the wire with the transverse mid-thickness across-the-width lamination involved the simultaneous lateral and transverse propagations of the initiated flat fracture frontward and backward through the wire's thickness and upward and downward through the wire's width respectively on both the front and

the back sides of the transverse mid-thickness across-the-width lamination as shown in Figure 9(d).

The third fracture stage in the wire with the double inclined-end crack-like laminations involved the complete fracture of the front and back ligaments due to the continuous slant fracture propagation as shown in Figure 10(a). Conversely, the third fracture stage in the wire with the double straight-end crack-like laminations involved the transition of the single flat fracture in the middle ligament to positively inclined (/) slant fractures on each side of the flat fracture as shown in Figure 10(b). The third fracture stage in the wire with the lateral mid-width across-the-thickness lamination involved the continuous transverse upward and downward flat fracture propagations along the wire's width, and the transitions to negatively inclined slant fractures (\) at the front and back sides of the flat fracture along the wire's thickness above and below the lateral mid-width across-the-thickness lamination as shown in Figure 10(c). Similarly, the third fracture stage in the wire with the transverse mid-thickness across-the-width lamination involved the continuous transverse upward and downward flat fracture propagations along the wire's width, and the transitions to positively inclined (/) slant fractures at the front and back sides of the flat fracture along the wire's thickness as shown in Figure 10(d).

The fourth fracture stage in the wire with the longitudinal double inclined-end crack-like laminations involved the slant fracture initiation in the remaining middle ligament as shown in Figure 11(a). The fourth fracture stage in the wire with the double straight-end crack-like longitudinal laminations involved the propagation of the slant fractures as shown in Figure 11(b). The fourth fracture stage in the wire with the lateral mid-width across-the-thickness lamination involved the simultaneous transverse upward and downward flat fracture propagations along the wire's width, and the propagation of the negatively inclined slant fractures (\) at the outer front

and back regions of the wire along the wire's thickness as shown in Figure 11(c). Similarly, the fourth fracture stage in the wire with the transverse mid-thickness across-the-width lamination involved the simultaneous upward and downward transverse propagation of the flat fracture, and the propagation of the positively inclined lateral slant fractures at the outer front and back regions of the wire along the wire's thickness as shown in Figure 11(d).

The fifth fracture stage in the wire with the double inclined-end crack-like longitudinal laminations involved the continuous propagation of the slant fracture in the remaining middle ligament as shown in Figure 12(a). The fifth fracture stage in the wire with the double straight-end crack-like longitudinal laminations involved the continuous propagation of the slant fracture in the middle ligament and a simultaneous two flat fracture initiations, each at the centers of the front and back ligaments as shown in Figure 12(b). At the fifth fracture stage in the wire with the lateral mid-width across-the-thickness lamination, the simultaneous transverse upward and downward propagation of the flat fracture along the wire's width and the propagation of the negatively inclined slant fractures (\) at the outer front and back regions of the wire along the wire's thickness have extended to the surfaces of the wire and are now visible in the meshed wire model as mid-thickness flat and mid-width slant fractures as shown in Figure 12(c). Similarly, at the fifth fracture stage in the wire with the transverse mid-thickness across-the-width lamination, the transverse upward and downward propagation of the flat fracture along the wire's width and the propagation of the positively inclined lateral slant fractures at the outer front and back regions of the wire along the wire's thickness have extended to the surfaces of the wire and are now visible in the meshed wire model as transverse flat fractures at the front and back sides of the transverse mid-thickness across-the-width lamination and as mid-width slant fractures as shown in Figure 12(d).

The complete fracture of the wires with the longitudinal double inclined-end, the lateral mid-width across-the-thickness lamination and the transverse mid-thickness across-the-width crack-like laminations occurred at the sixth fracture stage as shown in Figures 13(a), (c) and (d) respectively. The sixth fracture stage of the wire with the longitudinal double straight-end crack-like longitudinal laminations involved the propagation of the flat and slant fractures in the middle ligament, and the flat to slant fracture transition in the two outer ligaments of the wire as shown in Figure 13(b). As shown in Figure 14, the seventh, eighth and ninth fracture stages of the wire with the longitudinal double straight-end crack-like laminations involved the propagation of the slant fractures in the front, the middle and the back ligaments (Figure 14(a)), the complete fracture of the middle ligament (Figure 14(b)) and the simultaneous complete fracture of the front and back ligaments (Figure 14(c)) respectively. The middle ligament fractured first because fracture initiation and propagation stated in the middle ligament which was partially fractured long before the fracture initiations in the thicker front and back ligaments.

The predicted fracture shape exhibited by the wire with the longitudinal single straight-end crack-like lamination shown in Figure 15(c) agrees with the second fracture shape exhibited by the laboratory/field-fractured wires presented in the fractographic failure analysis report of USBR [12] shown in Figures 15(d). This result demonstrates that the section of the Jordan Aqueduct pre-stressed concrete pipe pre-stressing wires wire which exhibited the second fracture shape (Figures 15(d)) had a single straight-end lamination and establishes that not all the fractured Jordan Aqueduct pre-stressed concrete pipe pre-stressing wires had double/two offsetting and overlapping laminations as reported by USBR [12]. It also demonstrates that not all fractures occurred at the cross sections where a crack terminated and another originated as reported by USBR [12] as fractures also occurred at the cross sections of Jordan Aqueduct pre-

stressed concrete pipe pre-stressing wires with a single straight-end lamination. The predicted fracture shape exhibited by the wire with the double inclined-end crack-like laminations shown in Figure 15(e) agrees with the first fracture shape exhibited by the field and laboratory-fractured Jordan Aqueduct pre-stressed concrete pipe pre-stressing wires shown in Figures 15(f)) and is completely different from the predicted fracture shape exhibited by the wire with the double straight-end crack-like longitudinal laminations in Figure 14(c). This demonstrates that the section of the Jordan Aqueduct pre-stressed concrete pipe pre-stressing wires that exhibited the first field-and experimental fracture shape (Figure 15(f)) had two laminations with inclined-ends and not laminations (single or double) with straight-ends. Also, the USBR [12] concluded that the failure of the wires which exhibited the first fracture shape (Figure 15(f)) which has been established by FE to be the wires with the double inclined-end crack-like longitudinal laminations (Figure 14(e)) were caused by overloading of the wire as the metal tongue/filament carried a "little load". To the authors understanding, this conclusion suggests that the metal tongue referred to as the middle ligament in the FE model fractured first as it has a lower load-carrying capacity than the front and back ligaments. However, as revealed by the FE failure analysis, the front and back ligaments fractured first (Figure 10(a)) and fracture initiation in the metal tongue/middle ligament (Figure 11(a)) only started after the complete fracture of the front and back ligaments. This demonstrates that the metal tongue still had some load carrying ability while the crack propagated through it (Figure 12(a)) before its final failure as shown in Figure 13(a) long after the failure of the thicker front and back ligaments. Thus, through FE failure analysis, the types of crack-like laminations that were present in the sections of the wire that exhibited the first and second field and laboratory fractured shapes, and their fracture sequences, which were not distinguished in the report of USBR [12] have been identified.

At a glance, looking at the combination of the two slant fractures and the opening at the location of the lamination which seemingly looks like a flat fracture at the centre of the USBR [12]'s reported field and experimental fractured wire in Figure 15(d), a failure analyst could easily conclude that the fracture shape in Figure 15(d), is a cup and cone fracture. However, on the basis of the FE predicted fracture shape for the wire with the single straight-end crack-like lamination (Figure 15(c)) which aggress well with the field and experimental fracture shape in Figure 15(d) described by the authors in their earlier paper as a "V-shaped fracture with an opening at the bottom of the V where the single straight-end crack-like lamination is located" (see Adewole and Bull, (2014b), the fracture shape in Figure 15(d) can neither be described as a cup and cone fracture nor a cup and cone fracture with sharp tongue as reported by the USBR [12]. On the basis of the FE predicted fracture processes culminating into the formation of the fracture shape exhibited by the wire with the single straight-end crack-like longitudinal lamination (Figure 15(c)) hereinafter referred to simply as an "open–V" fracture presented in the earlier work of the authours (see Adewole and Bull, [13]), the field and experimental fracture shape in Figure 15(d) differs from the cup and cone fracture. It differs from the cup and cone fracture in terms of its fracture sequence/stages, fracture morphology and its fracture shape as follows:

(1) The cup and cone fracture has a flat fracture at the centre of the whole wire (Figures 15(a) and (b)). Conversely, the "open-V" shaped fracture has an opening at the centre of the whole wire where the single straight-end crack-like lamination is located (Figure 15(c)).

(2) As reported by the authours in their earlier published work (see Adewole and Bull, [13]), the cup and cone fracture started with a single flat fracture initiation at the centre of the whole wire. Conversely, the "open-V" shaped fracture started with two simultaneous flat fracture initiations

at the centers of the front and back ligaments since the centre of the whole wire in the wire with the single straight-end crack-like lamination is an opening at the commencement of its fracture process.

(3) In the cup and cone fracture shown in Figures 15(a) and (b), the slant fracture on one side of the single flat fracture is positively inclined and the slant fracture on the other side of the single flat fracture is negatively inclined. Conversely, in the "open V" shaped fracture, the two slant fractures on the two sides of the flat fracture in the back ligament are both positively inclined (/), while the two slant fractures on the two sides of the flat fracture in the front ligament are both negatively inclined(\) (Figure 15 (c) and (d). None of the two slant portions of the cup and cone fracture has a flat fracture (Figures 15(a) and (b)) as they were completely formed by slant fracture propagations. Conversely, the two "seemingly" slant portions of the "open-V" shaped fracture have a flat fracture each (Figures 14(c) and (d)) as they were formed by flat to slant fracture propagations.

Similarly, the predicted fracture shapes exhibited by the wire with the double inclined-end crack-like longitudinal laminations (Figure 15(d)) and the wire with the double straight-end crack-like longitudinal laminations (Figure 14(c)) cannot be described as a cup and cone fracture with sharp tongue, as reported by USBR (1994). This is due to the fact that the predicted fracture sequences in the wire with the double straight-end crack-like longitudinal laminations (Figures 8(b), 9(b), 10(b), 11(b), 12(b), 13(b) and 14(a) to (c)) and that of the wire with the double inclined-end crack-like laminations (Figures 8(a), 9(a), 10(a), 11(a), 12(a) and 13(a), and their fracture shapes shown in Figures 14(c) and 15(e) respectively are completely different from the cup and cone fracture sequence and fracture shape. Although, the fracture process of the wire with the double straight-end crack-like longitudinal lamination consists of flat to slant fracture transitions in each

of the three ligaments, which is similar to the cup and cone fracture process, the two slant fractures on the two sides of the flat fractures in the back, middle and front ligaments are all positively inclined (/). The fracture process of the wire with the double inclined-end crack-like longitudinal laminations consists of entirely slant fracture propagations and has nothing in common with the cup and cone fracture process. The predicted fracture shape for the wire with the double straight-end crack-like longitudinal laminations which looks like a "W" shape with a slant middle line (instead of a horizontal middle line in regular "W") at the junction of the two "V" halves is hereinafter referred to as "slant-middle W " fracture shape. The predicted fracture shape for the wire with the double inclined-end crack-like longitudinal laminations which agrees with the field fractured wire shown in Figure 15(f) can better be described as a "zig-zag" shape rather than a cup and cone fracture with a metal tongue presented by USBR [12].

As shown in Figure 13(c), the fracture shape exhibited by the wire with the lateral mid-width across-the-thickness lamination consists of a lateral mid-width across-the-thickness flat section at the location of the lamination and sections above and below the lamination. The sections of the fracture surface above and below the lateral mid-width across-the-thickness lamination consist of a flat fracture perpendicular to the lateral mid-width across-the-thickness lamination covering approximately the middle half of the wire's thickness and negatively inclined slant fractures at the outer front and back edges of the wire's thickness. As shown in Figure 13(d), the fracture shape exhibited by the wire with the transverse mid-thickness across-the-width lamination consist of a transverse mid-width across-the-thickness flat section at the location of the lamination and sections on the front and back sides of the lamination. The sections on the front and back sides of the transverse/vertical mid-width across-the-thickness lamination consist of a flat fracture parallel to the transverse mid-thickness across-the-width lamination covering

approximately 1mm (14% of the wire's thickness) on the front and back sides of the lamination and positively inclined slant fractures at the outer edges of the wire's thickness.

The presence of the double overlapping and offsetting inclined-end crack-like laminations caused a 6.30% reduction in ultimate load and a 52.64% reduction in the displacement at ultimate load, while the single straight-end crack-like lamination and the double overlapping and offsetting straight-end crack-like longitudinal laminations did not have any significant reductions in the ultimate load (0.003% reduction) and the displacement at ultimate load (0.03% reduction) of the wires. The presence of the 2mm deep lateral mid-width across-the-thickness and transverse mid-thickness across-the-width laminations caused 6.27% and 13.12% reductions in the ultimate load and 49.77% and 67.85% reductions in the displacement at ultimate load of the wires respectively. These results demonstrate that irrespective of the lamination type, geometry or orientation, the presence of crack-like laminations causes a larger reduction in the displacements at which the wires attained the ultimate load than the reductions in the ultimate load itself. The results predicted for the wires with the longitudinal lamination(s) agree with USBR [12] experimental test results which revealed that of all the longitudinally cracked wire subjected to laboratory tensile testing, only one sample failed below the required minimum tensile strength. These results demonstrate that the presence of longitudinal crack-like laminations does not have a significant effect on the tensile strength of the wire. Although the reduction in the ultimate load of the wire by the presence of the longitudinal double inclined-end lamination is not very significant, based on the FE result, it can be concluded that the only wire with the tensile strength below the minimum value observed by the USBR [12] contained the longitudinal double inclined-end lamination.

The presence of the longitudinal single straight-end, longitudinal double overlapping and offsetting straight-end, longitudinal double overlapping and offsetting inclined-end, lateral across-the-thickness and transverse across-the-width laminations caused 16%, 6%, 70%, 64.46% and 77.17% reductions in the displacements at fracture of the wires. The results demonstrate that irrespective of the crack-like lamination type, geometry or orientation, the presence of crack-like laminations has the worst effect on the displacement at fracture and consequently on the ductility of the wire than on the ultimate load of the wire. The results predicted for the wires with the longitudinal lamination(s) agree with the reduced necking and reduced reductions in area of the longitudinally cracked wires reported by the USBR [12], as reduced necking and reductions in area translate to reductions in the displacement at fracture/ductility of the wire.

The higher reductions in the ultimate load and the displacements at fracture of the wires by the 2mm deep transverse mid-thickness across-the-width laminations compared with the reductions caused by the 2mm deep lateral mid-width across-the-thickness laminations are due to the fact that the wire with the transverse across-the-width laminations has a lower net-sectional area of 60mm^2 (i.e. (12 x 7) – (2x12) mm^2) compared with the 70 mm^2 (i.e. (12 x 7) – (2x7) mm^2) net-sectional area of the wire with the lateral mid-width across-the-thickness lamination. 2x12mm^2 and 2x7mm^2 are the areas of the transverse mid-thickness across-the-width and the lateral mid-width across-the-thickness laminations respectively.

The presence of the approximately 2mm combined length of the two inclined-ends (1mm long each) of the longitudinal double inclined-end laminations, the 2mm deep lateral mid-width across-the-thickness and transverse mid-thickness across-the-width laminations caused higher reductions in the ultimate load and the displacement at fracture of the wires than the much longer (15mm long) longitudinal single and double laminations. This is because the inclined-ends, the

transverse and the lateral laminations caused significant reductions in the cross-sectional area of the wires while the longitudinal straight-end laminations and the straight portions of the double incline-end laminations do not. The approximately 2mm combined length of the two inclined ends of the double inclined-end laminations, the lateral mid-width across-the-thickness and the transverse mid-thickness across-the-width laminations leave the wire with net-sectional areas of 60 mm^2, 70 mm^2 and 60 mm^2 respectively that are significantly lower than the 84mm^2 gross-sectional area of the wires, while the crack-like longitudinal laminations with infinitesimal thickness leaves the wire with a net-sectional area approximately equal to the gross-sectional areas of the wire.

6.0 Conclusion

In this paper, the predictions and analyses of the failures of flat wires typically used as tensile and/or pressure armour wires in flexible pipes manufacture with various lamination types (single and double), geometries (straight-end and inclined end) and orientations (longitudinal, lateral and transverse) conducted using finite element analysis are presented. The FE failure analyses cover the predictions and analyses of the failures of: notched pre-cracked wires with a surface lateral across-the-thickness crack-like lamination, wires with longitudinal double inclined-end laminations typically found in the fractured pre-stressing wires of the ruptured Jordan Aqueduct Pre-stressed Concrete Pipes; and wires with longitudinal double straight-end, lateral mid-width across-the-thickness and transverse mid-thickness across-the-width laminations. FE predicted fractured shape for the notched pre-cracked wire with lateral surface across-the-thickness crack-like lamination is validated with experimental results. FE predicted fracture processes and fracture shapes of wires with longitudinal crack-like laminations are compared with those in the

published fractographic failure analysis report of wires with similar longitudinal crack-like laminations.

FE failure analysis revealed that longitudinal crack-like laminations do not always act as stress concentrators as reported by USBR [12]. Only the notched pre-cracked wires with a surface lateral across-the-thickness crack-like lamination, the wires with the lateral mid-width across-the-thickness and the transverse mid-thickness across-the-width laminations with laminations that are perpendicular to the tensile load path; and the wire with the longitudinal inclined-end crack-like laminations with the inclined-ends at an angle to the tensile load path act as stress concentrators. Straight-end crack-like laminations (single or double) that are parallel to the load path do not constitute stress concentrators. FE failure analysis also revealed that fracture initiations do not always occur at the termini of the offsetting and overlapping longitudinal crack-like longitudinal laminations as reported by USBR [12]. Fracture initiation only occurs at the termini of inclined-end crack-like longitudinal laminations with the inclined end at an angle to the tensile load path. For wires with the single and double straight end crack-like laminations, fracture initiation occurs at the middle of the thinner/thinnest ligament. Furthermore, FE failure analysis revealed that only lamination-free wire exhibits cup and cone fracture as neither the fracture sequences/stages nor the fracture shapes exhibited by the wires with the single straight-end crack-like lamination, double overlapping and offsetting straight-end crack-like laminations and double overlapping and offsetting inclined-end crack-like laminations agrees with the well know cup and cone fracture sequence and fracture shape. The fracture shapes exhibited by the wires with single straight-end lamination, double overlapping and offsetting straight-end crack-like laminations and double overlapping and offsetting inclined-end crack-like laminations can

better be described as an “open V”, “slant-middle W” and “Zig-zag” fracture shapes respectively.

The wires with the lateral mid-width across-the-thickness lamination exhibits a combination of a transverse mid-thickness flat fracture covering approximately half of the wire’s thickness and perpendicular to the lateral mid-width across-the-thickness lamination, and negatively inclined slant fractures at the remaining outer edges of the wire’s thickness above and below the lateral mid-width across-the-thickness lamination. The wires with the transverse mid-thickness across-the-width lamination exhibits a combination of transverse flat fractures parallel to and on both sides of the transverse mid-thickness across-the-width lamination, and positively inclined slant fractures at the outer edges of the wire’s thickness on both the front and back sides of the transverse mid-thickness across-the-width lamination.

The presence of single and double straight-end crack-like laminations do not have any significant effects on the wire’s yield and ultimate loads, while the presence of double inclined-end, lateral mid-width across-the-thickness and transverse mid-thickness across-the-width crack-like laminations causes significant reductions in the wire’s ultimate load. The presence of crack-like laminations generally reduces the displacement at fracture of wires with the highest to the least reductions caused by the transverse mid-thickness across-the-width, the lateral mid-width across-the-thickness, the double inclined-end lamination, the double straight-end crack-like lamination and the single straight-end crack-like lamination. Irrespective of the crack-like lamination type, geometry or orientation, the presence of crack-like laminations has a worst effect on the displacement at fracture and consequently on the ductility of the wires than on the ultimate load of the wires. Consequently, since the commencement of fracture/fracture initiation depends largely on the displacement at fracture, it can be deduced that the failure of the Jordan Aqueduct

pre-stressed concrete pipes started with the failure of the pre-stressing wires with the double inclined-end crack-like laminations, followed by the failure of the pre-stressing wires with the double straight-end crack-like laminations, the wire with the single straight-end crack-like lamination and finally by the failure of the lamination-free wire. Thus, strain-based criteria that are based on the displacement at yield/yield strain, displacement/strain at the ultimate load and the displacement at fracture/fracture strain capacity of the wire could serve as a more appropriate parameter to assess the quality and the structural integrity of wires with crack-like laminations than the stress-based design that are based on yield load/ stress, ultimate load/stress and the fracture load/stress. The need to employ strain-based criteria for the quality assurance of wires and the structural design and integrity of wire-reinforced structures can be further justified based on the report of the USBR [12] which established that the Jordan Aqueduct pre-stressed concrete pipe pre-stressing wires did not fail by design errors as the wire failed at a stress well below their design strength. Consequently, it can be concluded that the Jordan Aqueduct pre-stressed concrete pipe pre-stressing wires failed not necessarily by the reduction in their ultimate strength/load but by the significant reduction in their displacement at fracture and ductility by the crack-like laminations.

The use of FE failure analysis for the analysis of the failure of wires with and without crack-like laminations conducted in this work revealed major differences and similarities between the fracture process (fracture initiation and propagation) and the identity of the fracture shapes of the wires with single and double crack-like laminations reported by USBR [12]. The use of FE failure analysis also provides a better understanding of the fracture behaviours of wires with the different crack-like lamination types found in the fractured pre-stressing wires of the ruptured Jordan Aqueduct Pre-stressed Concrete Pipes. This demonstrates the need to employ FE failure

analysis as a complementary and/or an alternative tool to the fractographic analysis of wires and other engineering structures/components generally. It demonstrates the need to employ FE failure analysis particularly in situations where the fracture marks required for the accurate fractographic failure analysis have been destroyed by post fracture events such as the corrosion of the fracture surface of the Jordan Aqueduct pre-stressed concrete pipe pre-stressing wires reported by the USBR [12].

References

[1] Vander Voort, G. F. "Visual Examination and Light Microscopy". ASM Handbook, Vol. 12: Fractography, 1987, ASM International, Materials Park, Ohio, pp91-165.

[2] Pardoen, T., Scheyvaertsa, F., Simara, A., Tekoglu, C and Onck P., 2010. Multiscale modeling of ductile failure in metallic alloys, Comptes Rendus Physique, Vol 11, 326–345.

[3] Besson, J., Steglich D, and Brocks W, 2001. Modelling of crack growth in round bars and plane strain specimens, International Journal of solids and structures, 38, 8259-8284.

[4] Scheider, I and Brocks, W, 2003. Simulation of cup–cone fracture using the cohesive model, Engineering Fracture Mechanics, Vol 70, pages 1943–1961.

[5] Anderson T. L. 2005. Fracture mechanics fundamentals and applications, Third edition. CRC press, Taylor and Francis Group, ISBN -10:0-8493-1656-1.

[6] Xue, Liang , 2007. Damage accumulation and fracture initiation in un-cracked ductile solids subject to triaxial loading, International Journal of Solids and Structures, Vol 44, Issue 16, 5163-5181.

[7] Tvergaard, V. and Needleman A, 1984. Analysis of the cup-cone fracture in a round tensile bar, Acta Metallurgica, Vol 32, Issue 1, 157-169

[8] Kim, Y and Chao Y.J, 2008. Numerical simulation of cup-cone 549 fracture in a round tensile bar,Proceedings of PVP2008, 2008 ASME pressure vessel and piping division conference, July 28-3, 2008, Chicago, Illinois, USA

[9] Chen, W. K. "*Linear Networks and Systems* (Book style)." Belmont, CA: Wadsworth, 1993, 123–135.

[10] Peet, S. and Wilde, A. (2001). "Laminations-origin, detection and assessment". Congreso Internacional de Ductos, 14–16 November, 2001, Merida Yucatan, Mexico.

[11] Smith, B. O.' Jenning, A. P. H. and Grimshaw, A. G. (1957). "A portable lamination detector for steel sheet." British Journal of Applied, 9(5) 191–193.

[12] United States Bureau of Reclamation. Pre-stressed Concrete Pipe Failure Jordan Aqueduct, Reach 3".All U.S. Government Documents (Utah Regional Depository) 1994. Paper 284. http://digitalcommons.usu.edu/govdocs/284

[13] Adewole, K. K. and Bull S. J. (2014). "Numerical Prediction of the Effect of Lamination Orientation on Fracture Behaviour of Wires for Civil Engineering Applications", Archive of Civil Engineering, 60(4), 389-400.

[14] Adewole, K. K and Bull, S. J. (2013). "Effectiveness of the reverse bending and straightening tests in detecting laminations in wires for civil engineering applications." Archive of Civil engineering, LIX(4), 423-439.

[15] Adewole, K. K. and Bull, S. J. (2013). "Prediction of tensile and fracture properties of cracked carbon steel wires using finite element simulation." Journal of Civil Engineering and Management, 20(1), 1-10.

[16] Adewole, K. K. (2014). "Appropriate Mesh Design for Predicting Complete Fracture Behaviour of Wires for Civil Engineering Applications". American Society of Civil Engineers Journal of Materials in Civil Engineering`, 26(12), 04014095-1-7.

[17] Adewole K. K. (2014). "Numerical prediction of the effects of longitudinal crack-like laminations on the tensile properties of wires." Journal of civil engineering and management, doi:10.3846/13923730.2014.914093, in press.

[18] Adewole, K. K. (2013). "Identification of Appropriate Micromechanical Fracture Model for Predicting Fracture Performance of Steel Wires for Civil Engineering Applications." Global Journal of Researches in Engineering: Civil and Structural Engineering, 2013, 13(3), 24-33.

[19] Bernauer, G., and Brocks, W. (2002). "Micromechanical modelling of ductile damage and tearing results of a European numerical round robin." Fatigue and Fracture of Engineering Materials and Structures, 25(4), 363 – 384

[20] Simulia, 2007." Abaqus documentation". Abaqus Incorporation, Dassault Systemes;

[21] Hooputra H., Gese H., Dell H. and Werner H. A (2004). "Comprehensive failure model for crashworthiness simulation of aluminum extrusions". International Journal of Crashworthiness, 9(5), 449–64

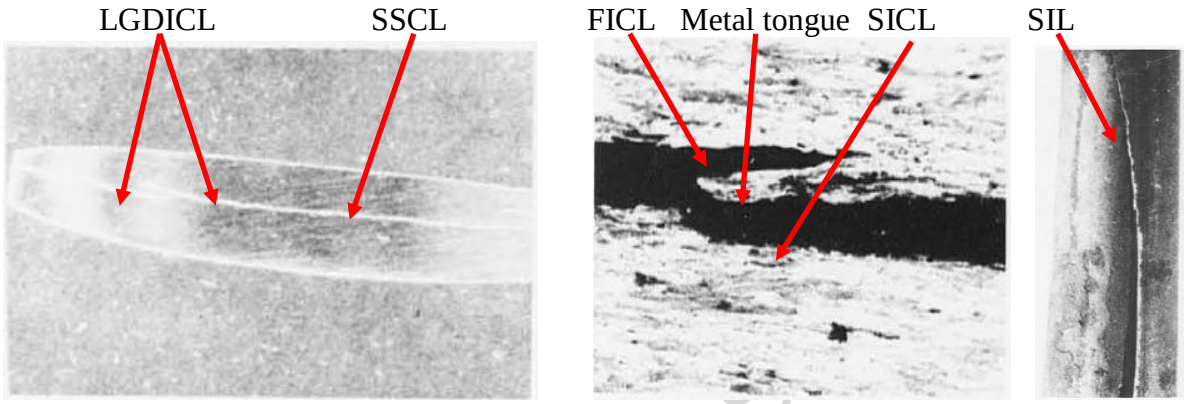

Figure 1: Photomacrograph of a short length of wire (a) Longitudinal double overlapping and offsetting inclined-end crack-like laminations (LGDIECL) and Longitudinal single straight-end crack-like laminations (LGSSECL), about 3X; (b) First inclined-end crack-like lamination (FICL), second inclined-end crack-like lamination (SICL), and metal tongue between overlapping and offsetting crack-like laminations, about 200X). (c) Single inclined-end lamination (SIL), about 9X (U. S. Bureau of Reclamation [12].

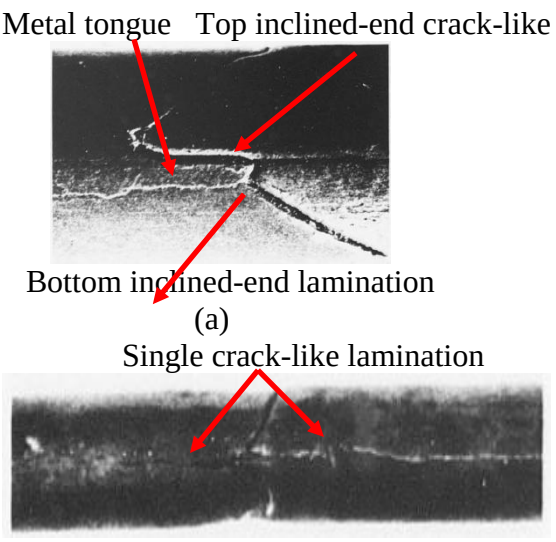

Figure 2(a) Field and laboratory fracture shapes of pre-stressing wires with crack-like laminations (US Bureau of Reclamation, 1994). (a) First fracture shape described as cup and cone failure with a metal tongue; (b) Second fracture shape unidentified by USBR [12].

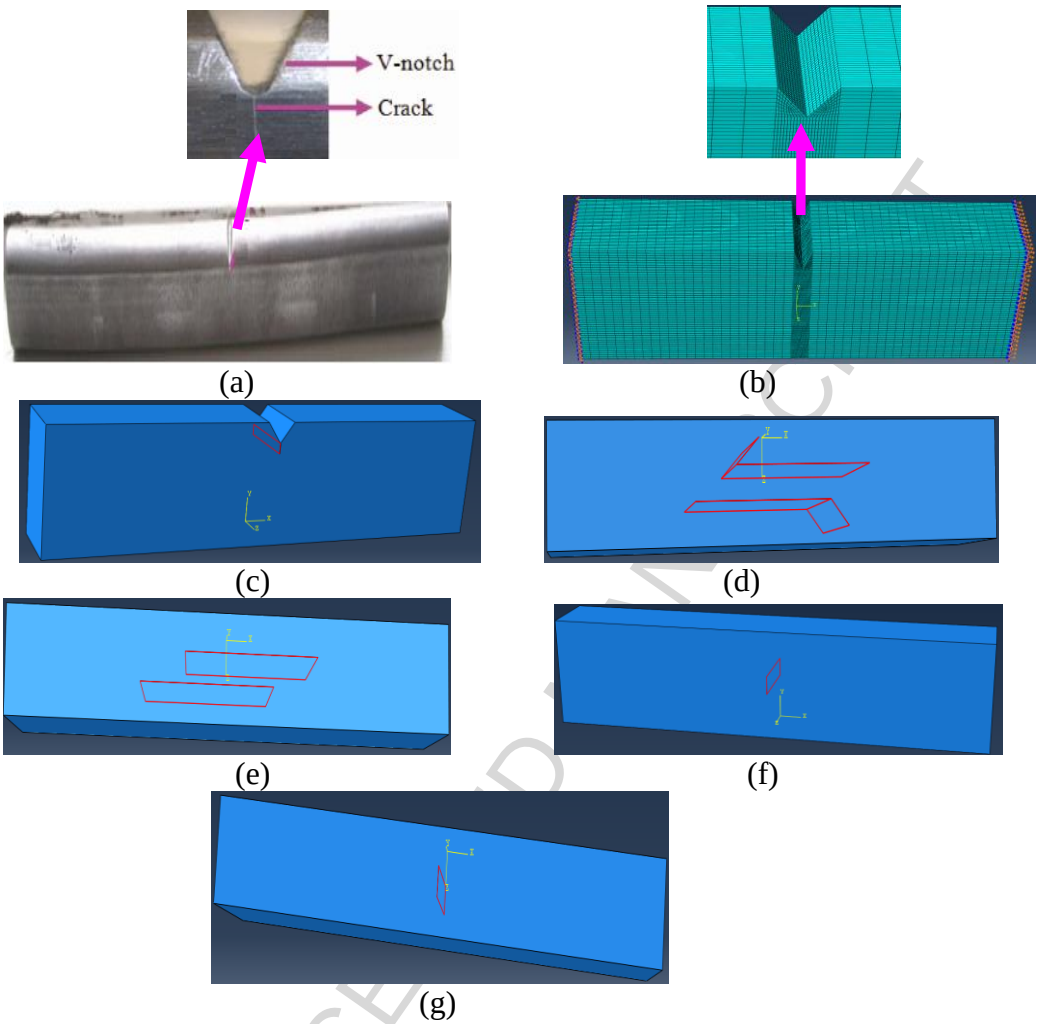

Figure 3: Experimental and FE models of wires with various crack-like laminations: (a) Experimental notched pre-cracked wire; (b) Meshed model of notched pre-cracked wire; (c) Unmeshed model of notched pre-cracked wire (d) Model of wire with double inclined-end crack-like laminations; (e) Model of wire with double straight-end crack-like laminations; (f) Model of wire with lateral mid-width across-the-thickness lamination; (g) Model of wire with transverse mid-thickness across-the-width lamination.

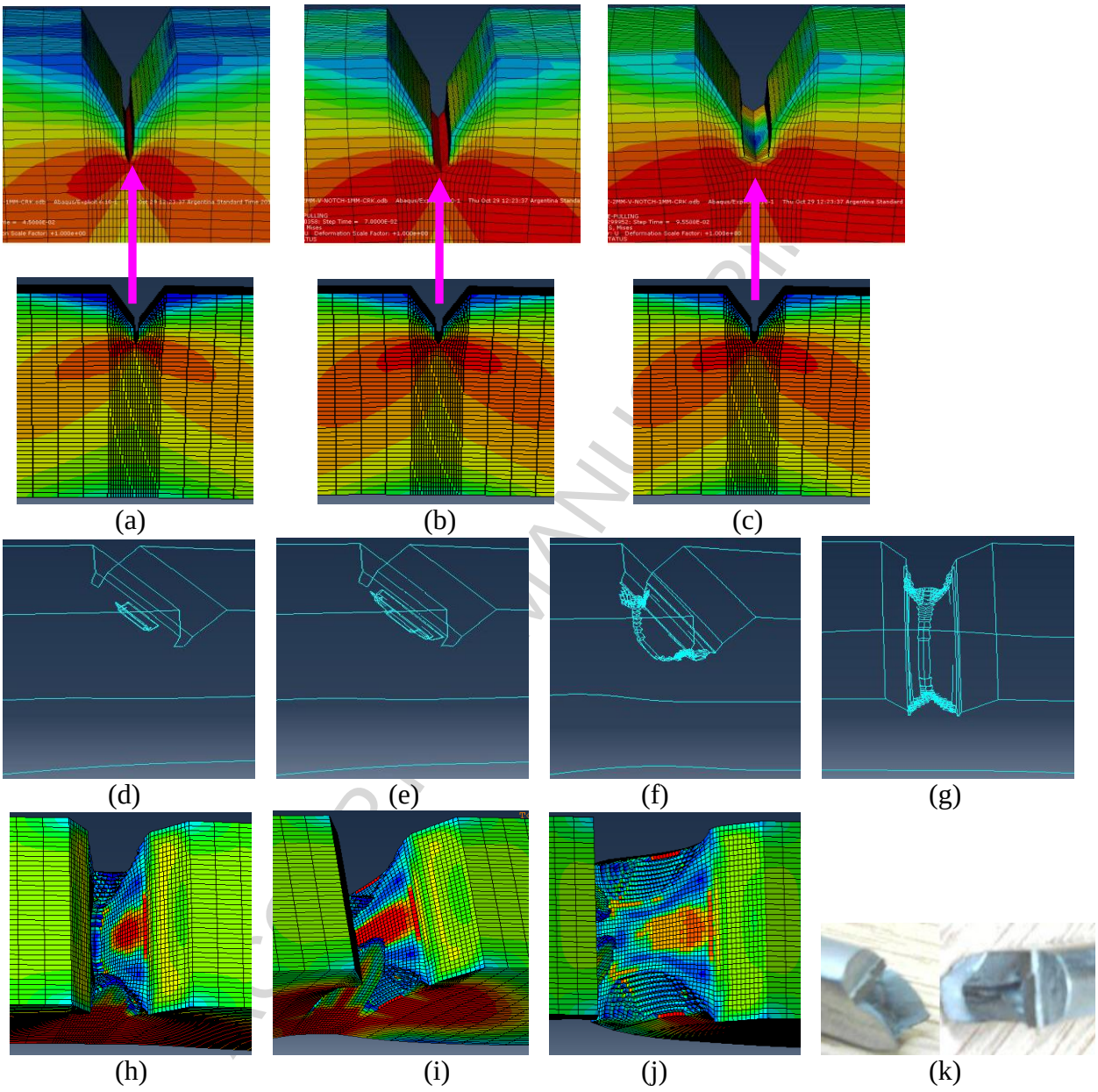

Figure 4. FE predicted fracture stages and experimental fractured shape of notched pre-cracked wire specimen: (a) End of elastic deformation; (b) At ultimate tensile strength; (c) at the end of the necking process; (d) Fracture stage 1; (e) Fracture stage 2; (f) Fracture stage 3; (g) Fracture stage 4; (h) Fracture stage 5 (i) Fracture stage 6 (j) Fracture stage 7; (k) Experimental fracture shape.

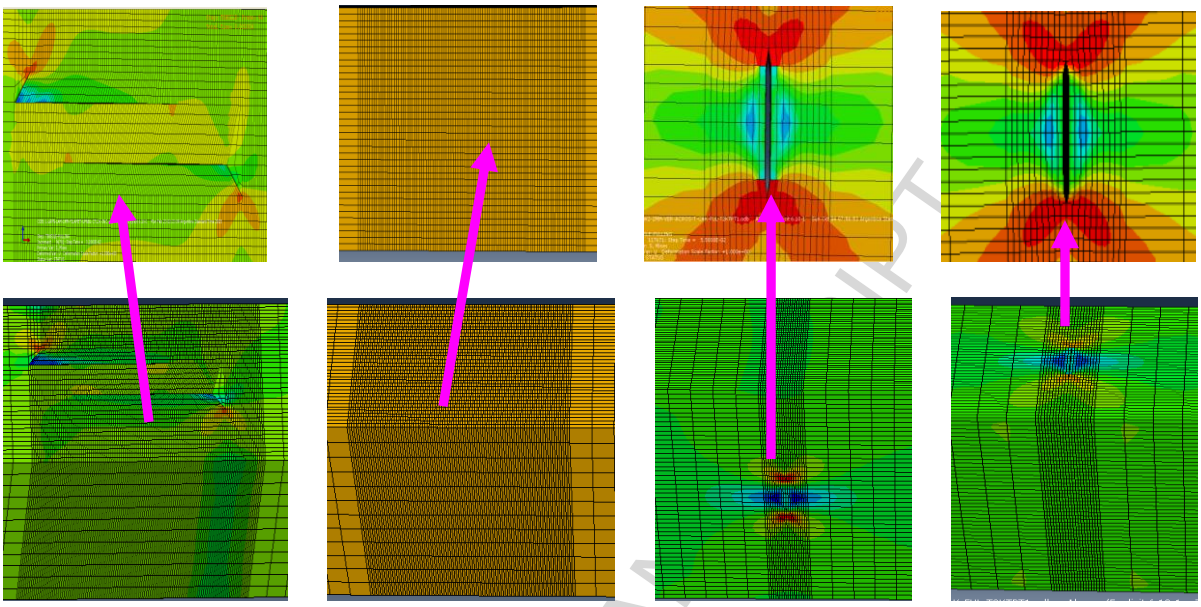

(a) (b) (c) (d)

Figure 5. Deformed shapes prior to yielding: (a) Wire with longitudinal double inclined-end laminations, (b) Wire with longitudinal double straight-end laminations; (c) Wire with lateral across-the-thickness lamination; (d) Wire with transverse across-the-width lamination.

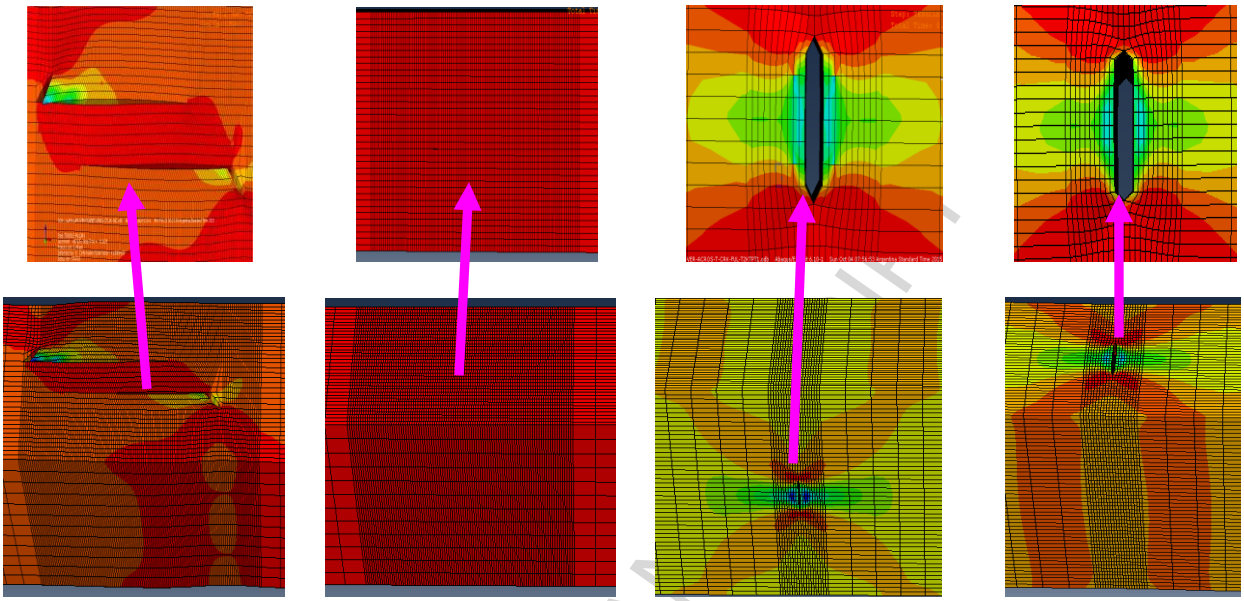

(a) (b) (c) (d)

Figure 6. Deformed shapes prior to yielding: (a) Wire with longitudinal double inclined-end laminations, (b) Wire with longitudinal double straight-end laminations; (c) Wire with lateral across-the-thickness lamination; (d) Wire with transverse across-the-width lamination.

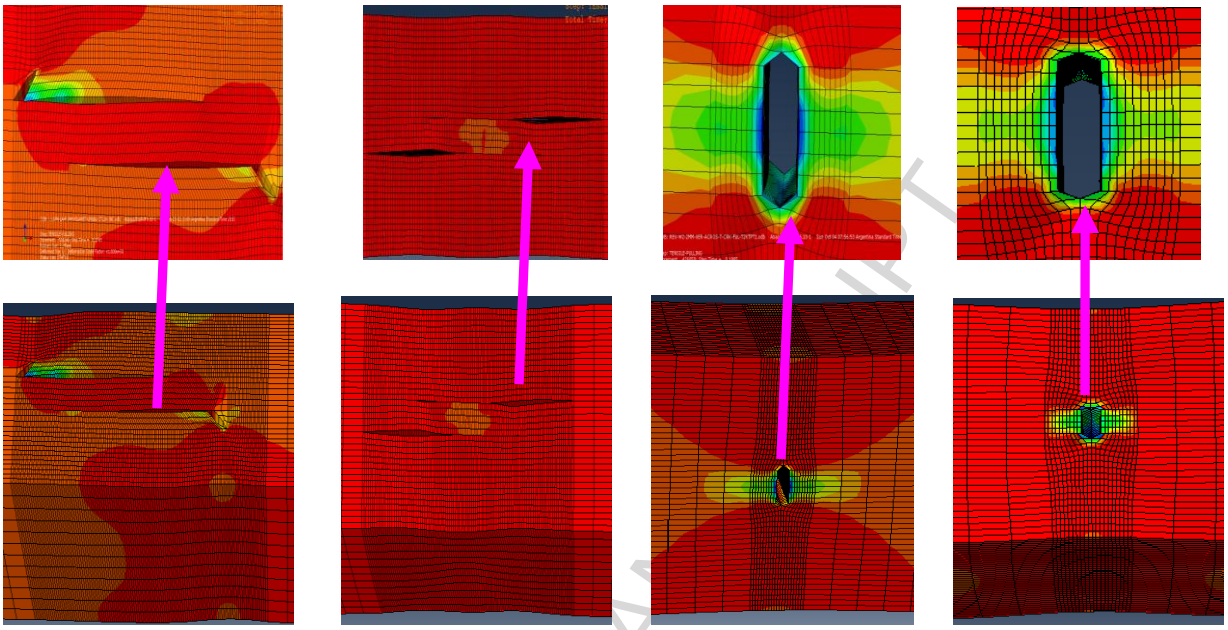

(a) (b) (c) (d)

Figure 7. Deformed shapes after necking: (a) Wire with longitudinal double inclined-end laminations, (b) Wire with longitudinal double straight-end laminations; (c) Wire with lateral across-the-thickness lamination; (d) Wire with transverse across-the-width lamination.

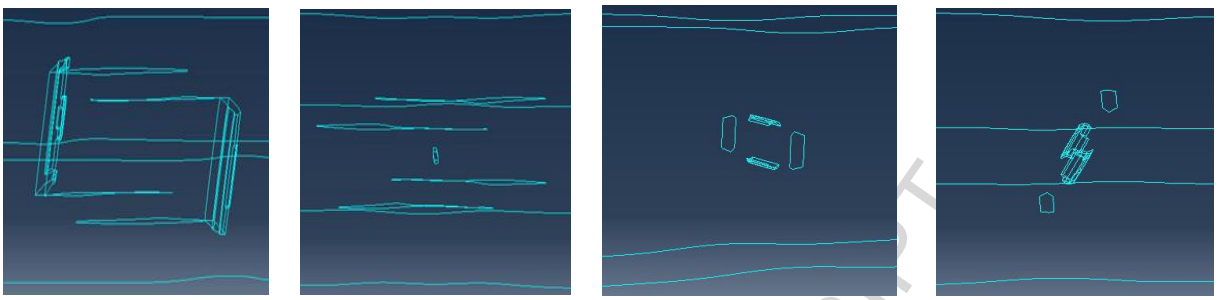

(a) (b) (c) (d)

Figure 8. Fracture process stage 1: (a) Wires with longitudinal double inclined-end crack-like laminations (b) Wire with the longitudinal double straight-end crack-like laminations. (c) Wire with lateral mid-width across-the-thickness lamination; (d) Wire with transverse mid-thickness across-the-width lamination.

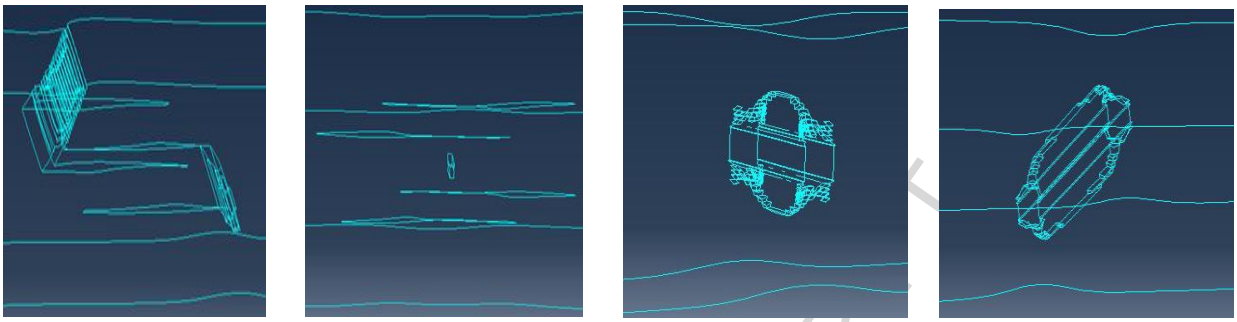

(a) (b) (c) (d)

Figure 9**.** Fracture process stage 2: (a) Wires with longitudinal double inclined-end crack-like laminations (b) Wire with the longitudinal double straight-end crack-like laminations. (c) Wire with lateral mid-width across-the-thickness lamination; (d) Wire with transverse mid-thickness across-the-width lamination.

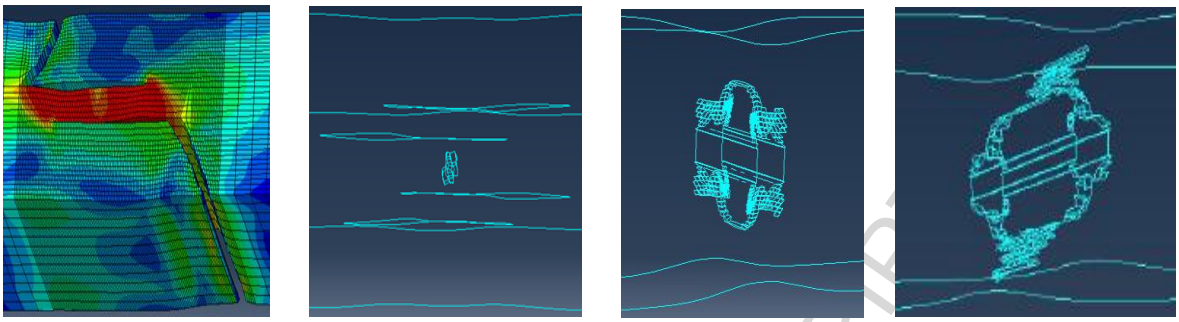

(a) (b) (c) (d)

Figure 10: Fracture process stage 3: (a) Wires with longitudinal double inclined-end crack-like laminations (b) Wire with the longitudinal double straight-end crack-like laminations. (c) Wire with lateral mid-width across-the-thickness lamination; (d) Wire with transverse mid-thickness across-the-width lamination.

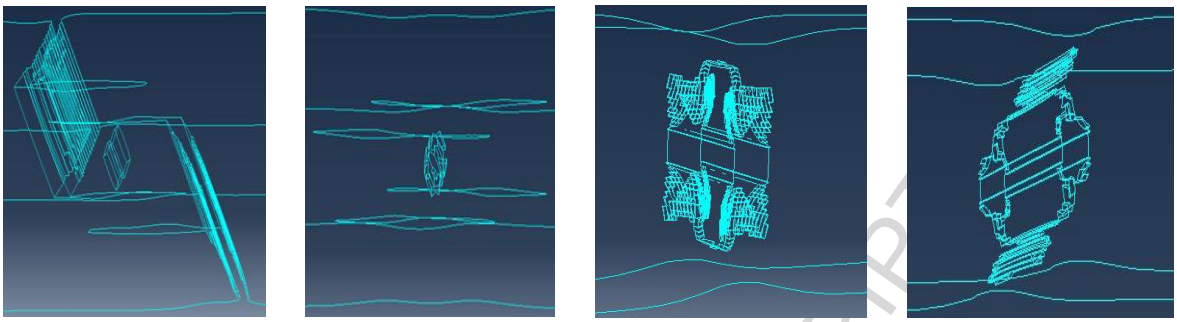

(a) (b) (c) (d)

Figure 11: Fracture process stage 4: (a) Wires with longitudinal double inclined-end crack-like laminations (b) Wire with the longitudinal double straight-end crack-like laminations. (c) Wire with lateral mid-width across-the-thickness lamination; (d) Wire with transverse mid-thickness across-the-width lamination.

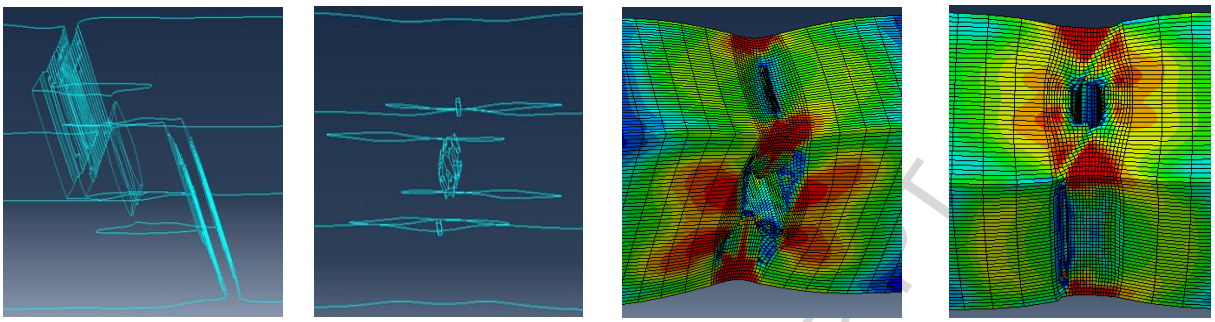

(a) (b) (c) (d)

Figure 12: Fracture process stage 5: (a) Wires with longitudinal double inclined-end crack-like laminations (b) Wire with the longitudinal double straight-end crack-like laminations. (c) Wire with lateral mid-width across-the-thickness lamination; (d) Wire with transverse mid-thickness across-the-width lamination.

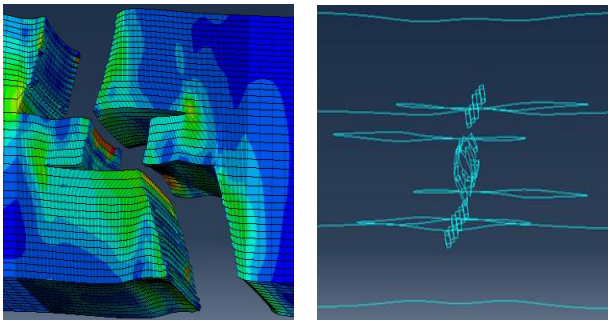

(a) (b)

Lateral mid-thickness
across-the-thickness lamination

Transverse mid-width
across-the-width lamination

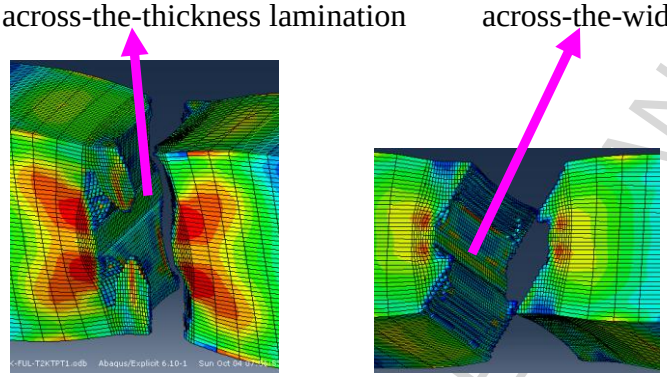

(c) (d)

Figure 13: Fracture process stage 6: (a) Wires with longitudinal double inclined-end crack-like laminations (b) Wire with the longitudinal double straight-end crack-like laminations. (c) Wire with lateral mid-width across-the-thickness lamination; (d) Wire with transverse mid-thickness across-the-width lamination.

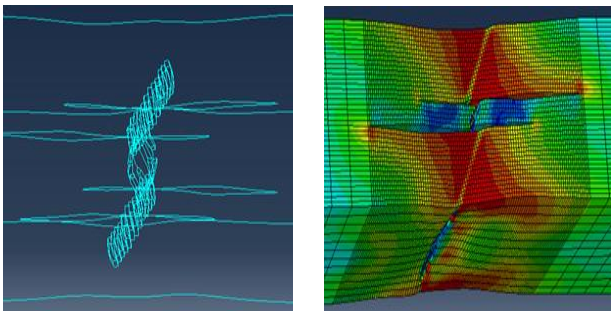

(a) (b)

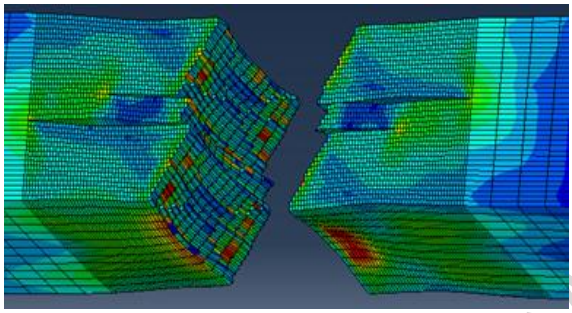

(c)

Figure 14: Last three fracture stages in wire with double straight-end crack-like laminations: (a) Seventh fracture stage; (b) Eight fracture stage; (c) Ninth fracture stage.

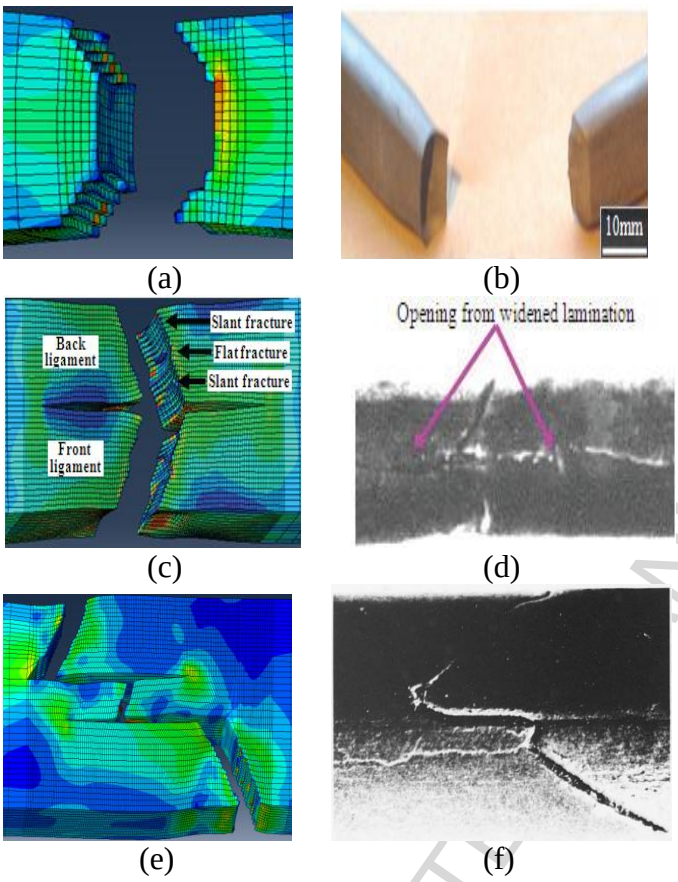

Figure 15. Experimental and FE predicted fracture shapes: (a) FE predicted fractured lamination-free wire (b) Experimental fractured lamination-free wire; (c) FE predicted fractured wire with single straight-end crack-like lamination (d) Experimental fractured wire with single straight-end crack-like lamination; (e) FE predicted fractured wire with double inclined-end crack-like laminations; (f) Experimental fractured wire with double inclined-end crack-like laminations.

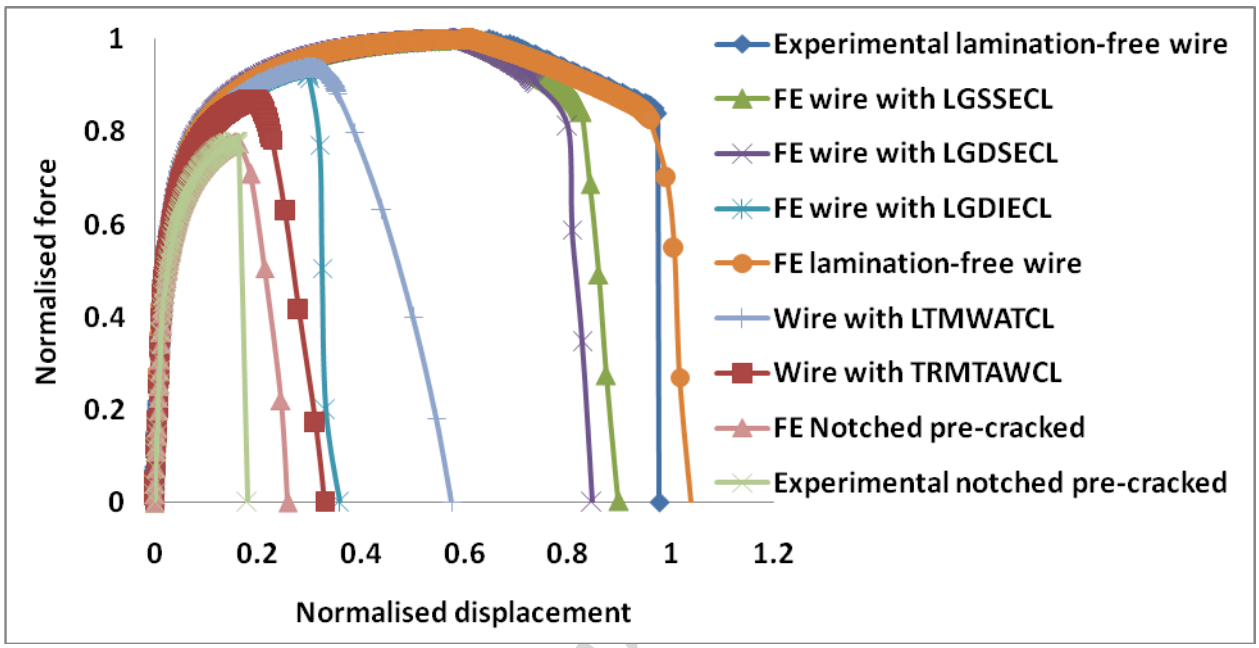

Figure 16: Force-displacement curves for lamination free wire, notched pre-cracked wires and wires with longitudinal double inclined-end crack-like laminations (LGDIECL), longitudinal double straight-end crack-like laminations (LGDSECL), Longitudinal single straight-end crack-like laminations (LGSSECL), lateral mid-width across-the-thickness (LTMWATCL), transverse mid-thickness across-the-width lamination (TRMTAWCL).

Highlights

Finite element failure analysis can compliment fractographic failure analysis

Fracture initiations do not always begin at termini of every crack-like lamination.

Fracture initiation only begins at the termini of inclined-end crack-like laminations

Finite element failure analysis useful where fracture markings have been distroyed